Experimental Demonstration of an IFFT/FFT Size Efficient DFT-Spread OFDM for Short Reach Optical Transmission Systems

Ming Chen, Xin Xiao, Zhaoran Rena Huang, Jianjun Yu, Fan Li, Qinghui Chen, and Lin Chen

***Abstract*—We experimentally demonstrate an IFFT/FFT size efficient discrete Fourier transform (DFT)-spread orthogonal frequency-division multiplexing (OFDM) based on complex-valued IFFT/FFT operations without Hermitian symmetry constraint at the input, for short-reach intensity-modulated and directly-detected optical fiber transmission systems. The only complex-valued IFFT-based OFDM has the similar peak-to-average power ratio (PAPR) and bit error rate (BER) performance, but with only half of the IFFT/FFT size as the conventional real IFFT-based OFDM. In this paper, the complex IFFT-based OFDM combined with DFT-spread technique is proposed and applied to reduce PAPR and IFFT/FFT size, and improve BER performance at the same time. The experimental results show that, with the help of PAPR reduction enabled by DFT-spread, more than 2-dB improvement in receiver sensitivity has been achieved after 20.62 km of single mode fiber transmission at a BER of 3.8×10^{-3} (7% hard-decision forward error correction threshold). In addition, by using the DFT-spread technique, the BER performance comparison between complex IFFT-based OFDM and real IFFT-based OFDM is also performed. The results show that, the BER performance of the former is slightly worse than the latter, but has lower hardware complexity and less power consumption due to the reduced IFFT/FFT size.**

***Index Terms*—Discrete Fourier transform-spread, direct detection, IFFT/FFT size efficient, optical orthogonal frequency division multiplexing.**

Manuscript received November 19, 2015; revised January 1, 2016; accepted February 10, 2016. Date of publication February 14, 2016; date of current version March 18, 2016. This work was supported in part by the U.S. National Science Foundation under Grant 1128540, in part by the National Natural Science Foundation of China under Grant 61325002 and Grant 61250018, and in part by the National High-Tech Research and Development Program (863 Program) of China under Grant 2015AA016904.

M. Chen is with the Department of Electrical, Computer, and System Engineering, Rensselaer Polytechnic Institute, Troy, NY 12180 USA, with the ZTE (TX) Inc., Morristown, NJ 07960 USA, and also with the College of Physics and Information Science, Hunan Normal University, Changsha 410081, China (e-mail: chenm10@rpi.edu).

X. Xiao and F. Li are with the ZTE (TX) Inc., Morristown, NJ 07960 USA (e-mail: xiao.xin@ztetx.com; fanli0809@gmail.com).

Z. R. Huang is with the Department of Electrical, Computer, and System Engineering, Rensselaer Polytechnic Institute, Troy, NY 12180 USA (e-mail: huangz3@rpi.edu).

J. Yu is with the Key Laboratory for Information Science of Electromagnetic Waves (MOE), Shanghai 200334, China, and also with the State Key Laboratory of ASIC and System, Fudan University, Shanghai 200334, China (e-mail: jianjun@fudan.edu.cn).

Q. Chen and L. Chen are with the Key Laboratory for Micro/Nano Optoelectronic Devices of Ministry of Education, College of Computer Science and Electronic Engineering, Hunan University, Changsha 410082, China (e-mail: chenqinghui0120@hnu.edu.cn; liliuchen12@vip.163.com).

Color versions of one or more of the figures in this paper are available online at http://ieeexplore.ieee.org.

Digital Object Identifier 10.1109/JLT.2016.2529429

I. Introduction

To meet the demand of ever-increasing bandwidth requirement in high-speed optical fiber communication [1], optical orthogonal frequency-division multiplexing (OOFDM) technique has high spectral efficiency (SE) and superior robustness to fiber dispersion, i.e., chromatic dispersion and polarization-mode dispersion, and is considered as one of the most promising solutions. By means of detection methods, OOFDM can be mainly classified into two types: direct-detection OOFDM (DDO-OFDM) [2]–[3] and coherent optical OFDM (CO-OFDM) [4]–[6]. CO-OFDM has higher receiver sensitivity at the expense of complex system configurations and this kind of OOFDM is very suitable for long-haul high-speed optical networks; while DDO-OFDM requires fewer components at transceiver than CO-OFDM, and is therefore more cost-effective. Recently, time- and wavelength-division multiplexed passive optical network (PON) has been identified by full service access network as the primary solution for next-generation PON stage 2 (NG-PON2) [7]. However, it is still realized by traditional on-off-keying (OOK) modulation, resulting in a low SE. Beyond NG-PON2, it is preferred to use the modulation formats with higher SE more than 1 bit/s/Hz instead of OOK modulation, and OFDM-based PON has become one of the most promising solutions for future optical access and data center networks [8]–[9].

It is well known that optical access networks are very cost-sensitive, and generally agreed that DDO-OFDM is much more suitable for cost-effective deployment compared to CO-OFDM [10]–[11]. Among the various DDO-OFDM systems, the real IFFT-based, i.e., the input vector of IFFT is constrained to have Hermitian symmetry (HS), and dc-biased optical OFDM (DCO-OFDM) is dominant in the current field programmable gate array (FPGA)-based real-time DDO-OFDM systems [12]–[18] due to its low complexity of hardware implementation. However, the IFFT/FFT size of this type of digital OFDM transceiver is not efficient due to the use of HS. Only half of subcarriers (SCs) can be used to carry quadrature amplitude modulation (QAM) mapped symbols. To address this problem, the I/Q channel separated baseband OFDM optical transmission using two orthogonal polarizations scheme has been proposed and experimentally demonstrated in a intensity-modulated and directly-detected (IMDD) system [19]. This scheme can achieve the doubled SE, but it has a complex system configuration. In addition, a FFT/IFFT size efficient method using complex IFFT/FFT operation was proposed and studied in asymmetrically clipped optical OFDM by numerical simulation [20]. This

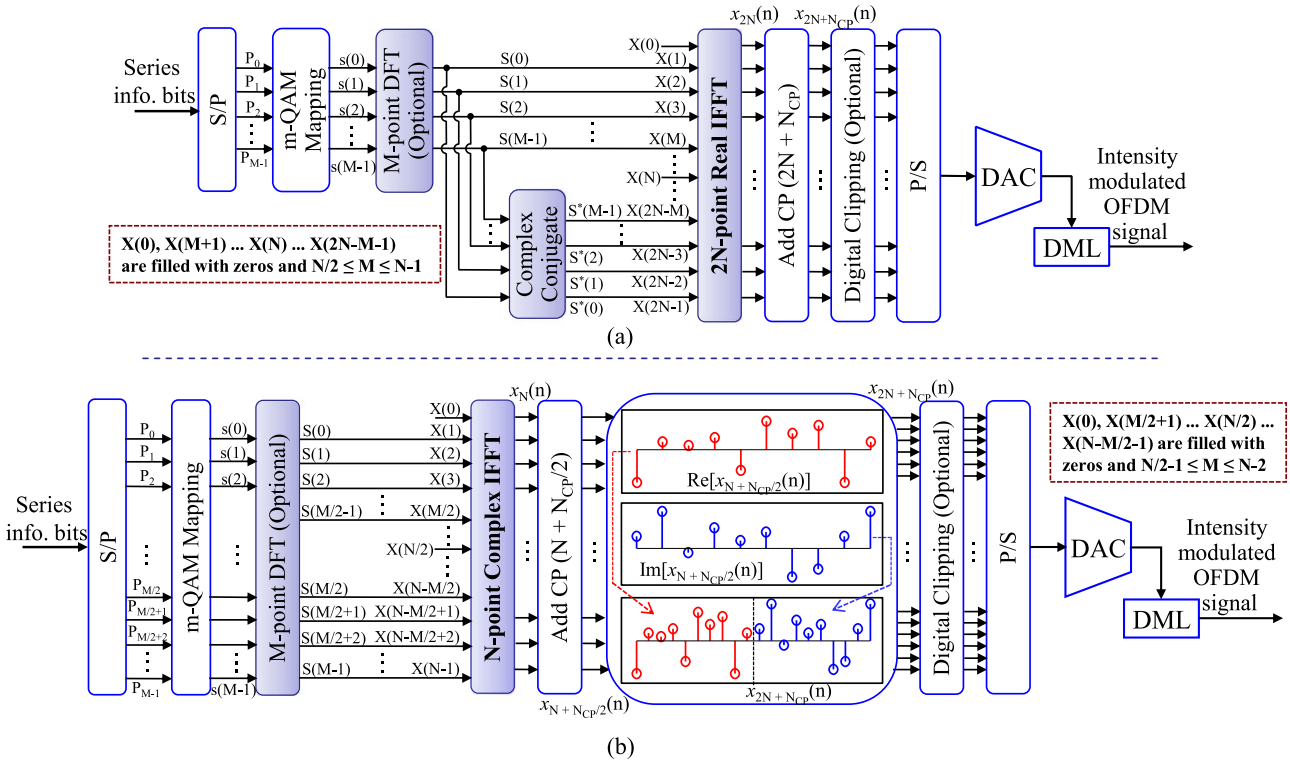

Fig. 1. Two types of DDO-OFDM transmitter based on (a) real IFFT and (b) complex IFFT.

method was also applied into DCO-OFDM, and only investigated by means of numerical simulation [21]. The results show that the hardware implementation complexity and power consumption can be largely reduced due to the reduced IFFT/FFT size, and the IFFT/FFT efficient OFDM signal has the similar bit error rate (BER) performance and peak-to-average power ratio (PAPR) as conventional real IFFT based DCO-OFDM. However, the high PAPR of the OFDM signal is still a problem for such DCO-OFDM systems. Especially for the generation of high QAM (e.g., 64-, 256- and 1024-QAM) encoded OFDM signals, it requires high-resolution digital-to-analog converters (DACs) and analog-to-digital converters (ADCs), and suffers from the nonlinearity of the electric and optical components (e.g., RF amplifier and optical fiber). Recently, discrete Fourier transform (DFT) spread technique with the advantages of PAPR reduction as well as BER performance improvement [22]–[23], has been experimentally demonstrated in OOFDM systems.

In this paper, the IFFT/FFT size efficient method combined with PAPR reduction enabled by DFT-spread technique is proposed for DCO-OFDM systems. The transmission performance of the proposed optical OFDM signal is experimentally investigated in 20.62-km single mode fiber (SMF) IMDD system using a commercial directly-modulated laser (DML).

II. Operation Principle

Two types of DDO-OFDM transmitter are plotted in Fig. 1. The conventional real IFFT based OFDM modulation with DFT-spread technique is shown in Fig. 1(a). The high-speed series information bits are first converted into M parallel channels,$\mathrm{P}_0, \mathrm{P}_1, \mathrm{P}_2, \ldots, \mathrm{P}_{\mathrm{M}-1}$, and then mapped into M complex QAM symbols, $\mathrm{s}(0), \mathrm{s}(1), \mathrm{s}(2), \ldots, \mathrm{s}(\mathrm{M}-1)$. Every mapped symbol can be spread into M SCs by employing M-point DFT operation. To realize the M DFT-spread symbols, $\mathrm{S}(0), \mathrm{S}(1), \mathrm{S}(2), \ldots, \mathrm{S}(\mathrm{M}-1)$, OFDM modulation, where M is an integer with the range of [N/2, N-1], and achieve the real-valued outputs from 2N-point IFFT, the input vector of 2N-point IFFT is constrained to have HS, where input vector [X(2N-M), . . . , X(2N-2), X(2N-1)] of IFFT is the complex conjugate of [S(M-1), . . . , S(1), S(0)]. After IFFT operation, $\mathrm{N_{CP}}$-point cyclic prefix (CP) is taken from the end of IFFT output is appended in front of it. Digital clipping is a simple way to reduce PAPR, and is commonly used in FPGA-based real-time OOFDM systems [9], [12], [15]. However, the clipping causes distortion of the transmitted OFDM signal and introduces clipping noise. In this paper, the BER performance comparison among unclipped, clipped and DFT-spread OFDM signals will be performed for both conventional OFDM and IFFT/FFT size efficient OFDM. At last, the $2\mathrm{N} + \mathrm{N_{CP}}$ parallel real-valued samples are converted to series ones for DAC, and then the converted baseband OFDM signal are used to drive an intensity modulator, for example, DML, to generate IM optical OFDM signal. After SMF link transmission, the optical OFDM signal is directly detected by one photo-detector (PD). The recovered baseband signal is then sampled by an ADC. The receiver digital signal process (DSP) functions mainly include symbol timing synchronization, CP removal, 2N-point FFT, channel estimation and equalization and QAM de-mapping.

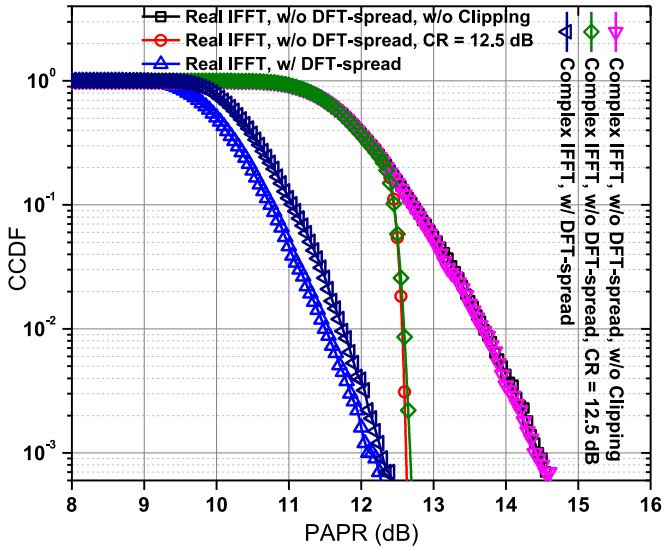

Fig. 2. CCDFs versus PAPR for six types of OFDM signal.

The IFFT size efficient OFDM modulation combined with DFT-spread technique is illustrated in Fig. 1(b). The M QAM-mapped or DFT-spread symbols, where M is an integer from [N/2-1, N-2], are allocated into M SCs (i.e., [S(0), S(1), . . . , S(M/2-1), S(M/2), S(M/2+1), . . . , S(M-1)] -> [X(1), X(2), . . . , X(M/2), X(N-M/2), X(N-M/2+1), . . . , X(N-1)]). In this way, only N-point complex IFFT can be used to realize OFDM modulation. After $N_{CP}/2$-point CP addition and/or digital clipping operations, the $N + N_{CP}/2$ complex OFDM samples, $x_{N+N_{CP}/2}(n)$, $n \in [0, N + N_{CP}/2 - 1]$, are separated into $N + N_{CP}/2$ real parts and $N + N_{CP}/2$ imaginary parts. Then a total of $2N + N_{CP}$ parallel real-valued samples, $x_{2N+N_{CP}}(n)$, $n \in [0, 2N + N_{CP} - 1]$ are digitally clipped and converted to series ones. At receiver DSP functions, $N + N_{CP}/2$ real parts and $N + N_{CP}/2$ imaginary parts are combined into $N + N_{CP}/2$ complex-valued samples after symbol timing synchronization and N-point FFT is performed after CP removal.

According to above-mentioned, as the length of the IFFT size efficient OFDM symbol is doubled after separation operation while the IFFT size is reduced by half from 2N-point to N-point, the SE of the IFFT size efficient OFDM signal is the same as the conventional one.

Fig. 2 shows the complementary cumulative distribution functions (CCDFs) as a function of PAPR for six types of digital OFDM signal with two-times time-domain interpolation. Each CCDF curve is calculated from 10 000 continuous OFDM symbols. The sizes of the real IFFT and complex IFFT are 4096 and 2048, respectively. And the number of the data-carrying SCs is 1640 for the both cases. The DFT-spread disabled and unclipped complex IFFT-based and real-valued OFDM (we call it as "complex IFFT-based OFDM") signal, exhibits the same PAPR as that of the conventional real IFFT-based OFDM (called "real IFFT-based OFDM") signal; while the PAPR of DFT-spread technique enabled OFDM signals, at a CCDF of 1×10^{-3}, can be reduced by more than 2-dB for both complex IFFT and real IFFT-based OFDM. A similar PAPR between complex IFFT and real IFFT-based OFDM, by using DFT-spread technique, are also observed in Fig. 2. Moreover, the PAPRs of only clipped OFDM signals at an optimal digital clipping ratio (CR) [24] of 12.5-dB are also presented for comparison.

III. Experiment Setup

The experimental setup for the investigation of transmission performance of the proposed DFT-spread enabled and complex IFFT-based OFDM signal and other five types of OFDM signal, i.e., DFT-spread enabled and real IFFT-based, clipped complex IFFT and real IFFT-based, unclipped complex IFFT and real IFFT-based OFDM signals, are shown in Fig. 3. For OFDM modulations, M is 1640, modulation format is 64-QAM, and IFFT sizes of real IFFT and complex IFFT-based OFDM are 4096 and 2048, respectively. The QAM mapped 1640 symbols or 1640 DFT outputs if DFT-spread is enabled, are assigned to the corresponding 1640 SCs according to the methods shown in Fig. 2. By this way, the six types of OFDM signal have similar spectrum shapes in frequency-domain. In addition, large IFFT/FFT size can be used to improve the robustness to the inter-symbol interference (ISI) [25] due to channel bandwidth limitation (e.g., roll-off effect of DAC). CP with different lengths of 0, 1/1024, 1/512, 1/256, 1/128, 1/64, 1/32, 1/16, 1/8 and 1/4 IFFT size is used for all OFDM signals to study the impact on transmission performance. The OFDM signals are clipped at a CR of 12.5-dB if the digital clipping is used. To improve the quality of the DAC converted baseband signal converted, 2-times interpolation is implemented after parallel-to-serial conversion. Here, an OFDM frame consists of one training sequence (TS) and 180 data-carrying OFDM symbols. The continuous OFDM frames are repeatedly generated by the arbitrary waveform generator (Tektronix AWG 7122C) operating at resolution of 10-bit and sample rate at 10-GS/s. As the result, the net rates are from 11.95 to 9.56-Gb/s as CP lengths are set from 0 to 1/4 IFFT size.

The OFDM signal generated from the AWG with an output voltage swing of 210-mV, is amplified by a RF amplifier (AMP, Mini-Circuits ZX60–43+) with a bandwidth of 4-GHz. The amplified signal is used to drive a commercial 1550-nm DML (Agilent 83430A) with 3-dB bandwidth of 2.5-GHz. The IM optical OFDM signal with a power of –1-dBm generated from the DML is boosted by an erbium-doped fiber amplifier (EDFA) up to 8-dBm. The noise figure of the EDFA is 5-dB. The optical spectra of optical carrier and IM OFDM signal at 2-dBm are shown in Fig. 3. The amplified optical signal is coupled into 20.62-km SMF. The SMF has an attenuation of 0.19-dB/km, and a dispersion of 17-ps/nm/km. At the receiver, the received optical signal is attenuated by a variable optical attenuator (VOA) with a low insertion loss (∼0.5-dB). An optical coupler with a power splitting ratio of 9:1 is placed in front of a 10-Gb/s PIN-PD with a responsivity of 0.8-A/W. The 10% power of received optical signal is used for power measurement, while the received signal with 90% power is directly detected by the PIN-PD to electrical baseband signal. Then the signal is sampled and stored by a digital storage oscilloscope (DSO, Tektronix TDS6804B) operating at resolution and sample rate

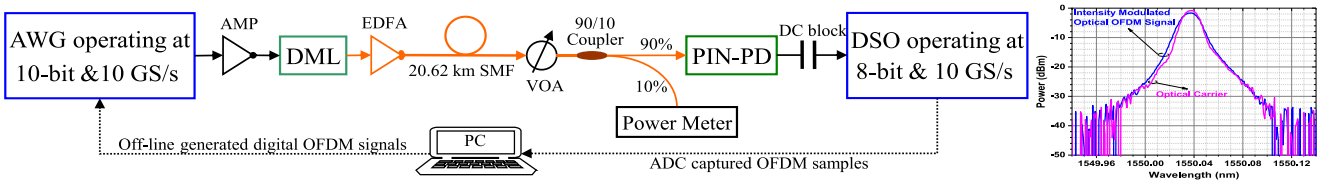

Fig. 3. Experimental setup of DML-based IMDD SMF transmission system.

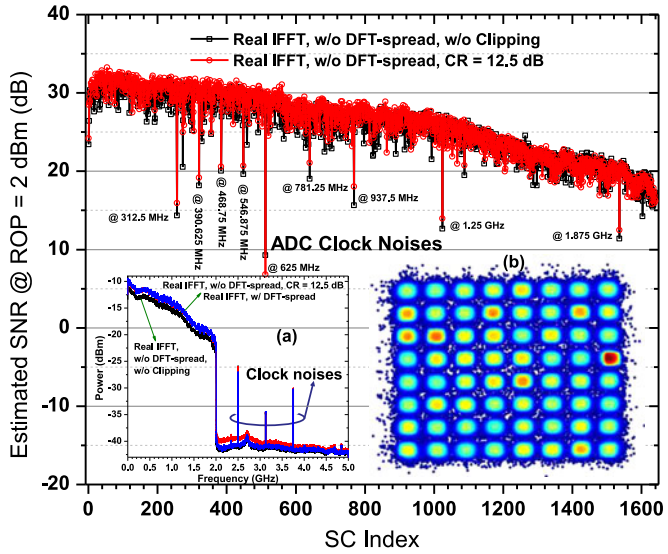

Fig. 4. Estimated SNR versus SC index for real IFFT-based OFDM (CP length = 0).

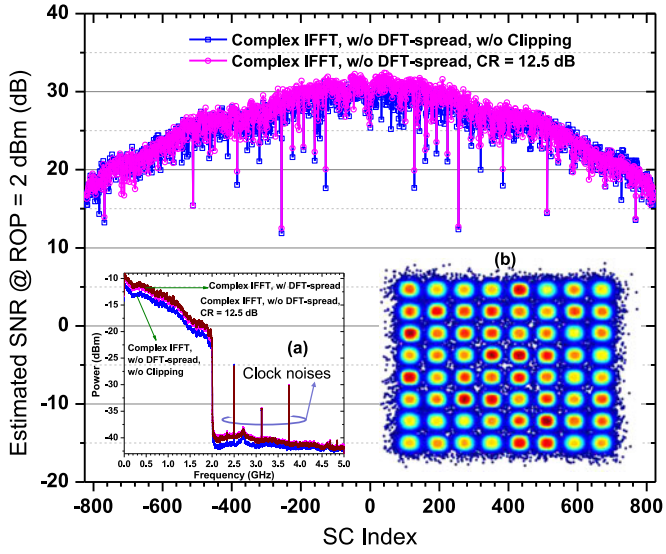

Fig. 5. Estimated SNR versus SC index for complex IFFT-based OFDM (CP length = 0).

of 8-bit and 10-GS/s after removing the Dc component using a dc block. The samples will be processed off-line by following steps: 2:1 down-sampling, TS-aided symbol timing synchronization, real parts and imaginary parts combination (only for complex IFFT-based OFDM signals), CP removal, FFT operation, TS-based single-tap channel estimation and equalization, IDFT operation (only for DFT-spread enabled OFDM signals), 64-QAM de-mapper, BER calculation and signal-to-noise ratio (SNR) estimation [27]. It should be mentioned that only one TS is used for both symbol timing synchronization and channel estimation, which can be found in our early work [18].

IV. Results and Discussions

For the six types of OFDM signal without CP after 20.62-km SMF transmission, at a received optical power (ROP) of 2-dBm, the estimated SNRs as functions of SC index and index of 1640-point IDFT output, are shown in Figs. 4, 5, and 6. As we can see from Fig. 4, there are some SNR-degraded SCs for real IFFT-based OFDM, which are mainly attributed into ADC clock noises [23], [26] located on these SCs. The SNR difference between high-frequency SCs and low-frequency SCs is up to more than 15-dB, which is mainly caused by bandwidth-limited devices such as the DAC, AMP and DML. The clipped OFDM signal has a little higher average power after DAC conversion due to its lower PAPR [see Fig. 4 (a)], it still shows that the clipped signal has a similar SNR performance as unclipped signal, which is mainly caused by the clipping noise. The uncentralized color-graded 64-QAM constellation of unclipped signal is also illustrated in Fig. 4(b).

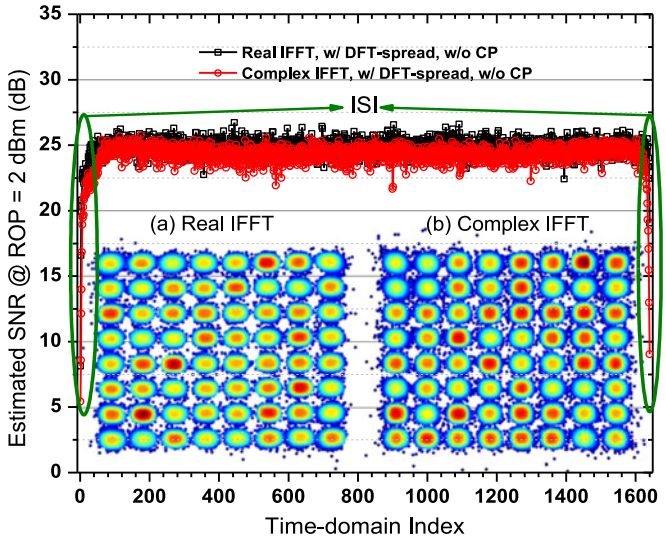

Fig. 6. Estimated SNRs versus time-domain index for two types of DFT-spread enabled OFDM (CP length = 0).

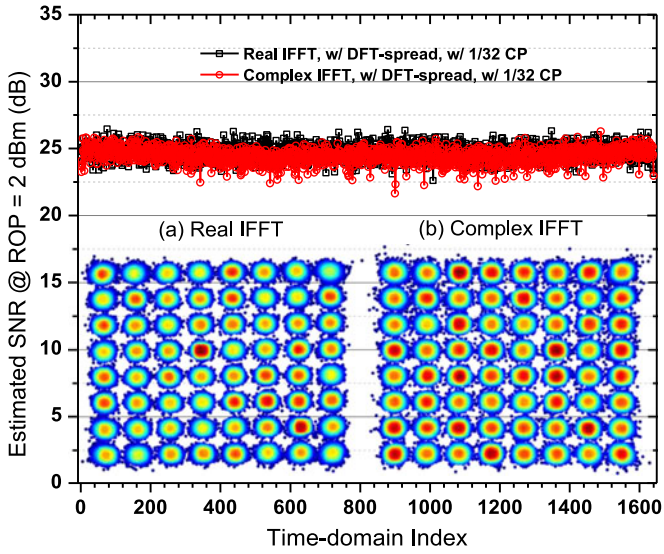

Fig. 7. Estimated SNRs versus time-domain index for two types of DFT-spread enabled OFDM (CP length = 1/32 IFFT size).

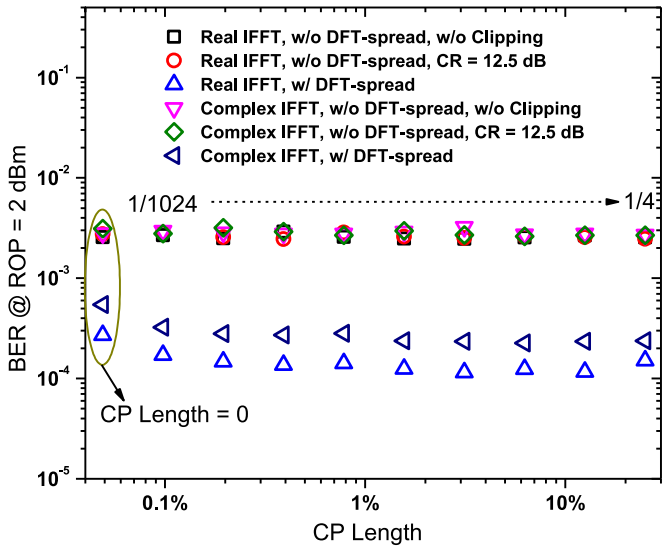

Fig. 8. Measured BER value versus CP length.

The estimated SNR as a function of SC index for unclipped and clipped complex IFFT-based OFDM signals are also shown in Fig. 5. The 1640 data-carrying SCs consist of 820 negative-frequency SCs and 820 positive-frequency SCs. As mentioned before, in real IFFT-based OFDM case, the bandwidth-limited devices (e.g., DAC, DML, and AMP) and ADC clock noises are also the reasons for degraded SNR performance on some SCs. The clipped signal has a fairly similar SNR performance and spectral shape [see Fig. 5(a)] as unclipped one, it is also observed for complex IFFT-based OFDM. The corresponding un-centralized 64-QAM constellation of unclipped signal is depicted in Fig. 5(b).

As DFT-spread-enabled OFDM signals have lower PAPR compared to which without using DFT-spread technique, the electrical average power of the AWG generated the corresponding OFDM signals is higher than that of only real IFFT or complex IFFT-based OFDM signal, as shown in Figs. 4(a) and 5(a). This fact will, to some extent, improve SNR performance of the recovered OFDM signal. In the case of CP length equals to zero, the estimated SNRs as functions of index of 1640-point IDFT output, here, we call it as "time-domain index," for the two types of DFT-spread enabled OFDM are shown in Fig. 6. It can be clearly seen that, the SNRs on both the beginning and ending of time-domain indexes are degraded due to the ISI caused by channel bandwidth limitation. As shown in Fig. 7, the CP with a length of 1/32 FFT size is applied. As a result, we can see the SNRs on the beginning and ending of time-domain index is significantly improved for the two types of DFT-spread enabled OFDM. Besides, the proposed complex IFFT-based and DFT-spread OFDM signal has slightly lower SNR performance than that of real IFFT-based and DFT-spread OFDM signal. The corresponding constellations for the two types of the OFDM signals without CP are shown in Fig. 6(a) and (b). Moreover, the more centralized constellation diagrams for the two types of CP appended OFDM signals are also shown in Fig. 7(a) and (b).

It is well known that, DFT-spread OFDM is a single-carrier-like transmission scheme, and more sensitive to ISI. An optimal length of CP should be appended in front of IFFT output to combat the ISI as well as guarantee high SE. The BER as a function of CP length for six types of OFDM signal at a ROP of 2-dBm, is depicted in Fig. 8. It shows that four types of DFT-spread disabled OFDM signals with CP length from 0 to 1/4 FFT size, have similar BER values around 3×10^{-3}; while the BER performance can be improved by about one order of magnitude when using the DFT-spread technique. Even though the two types of DFT-spread enabled OFDM signals are more sensitive to ISI, the BER can be improved if the CP with a length of 1/1024 FFT size is used for these two types of OFDM signal. Moreover, it also exhibits that the BER of the proposed complex IFFT-based and DFT-spread OFDM signal is only slightly higher than that of real IFFT-based DFT-spread one. One possible reason may be that the real IFFT-based DFT-spread OFDM with larger IFFT/FFT size has stronger robustness against ISI.

Fig. 9 shows the measured BER results as a function of ROP for six types of 11.9-Gb/s OFDM signal with a CP length of 1/1024 IFFT/FFT size, at optical back-to-back (ob2b) and 20.62-km SMF transmission cases. At low ROPs, the clipped OFDM signals have higher average power resulted from reduced PAPR, and they have a little better BER performances compared with those of unclipped ones. Although the clipped signals have almost the same of average power [see Figs. 4(a) and 5(a)] as DFT-spread enabled OFDM signals, the deeply degraded SNRs on some SCs make the BER performance worse than that of the two types of DFT-spread enabled OFDM signals. At a BER of 3.8×10^{-3}, which is the threshold of 7% hard-decision forward error correction, with the use of the two types of DFT-spread enabled OFDM signal, the receiver sensitivities can be improved by more than 2-dB, in contrast to that of the other four types of OFDM signal.

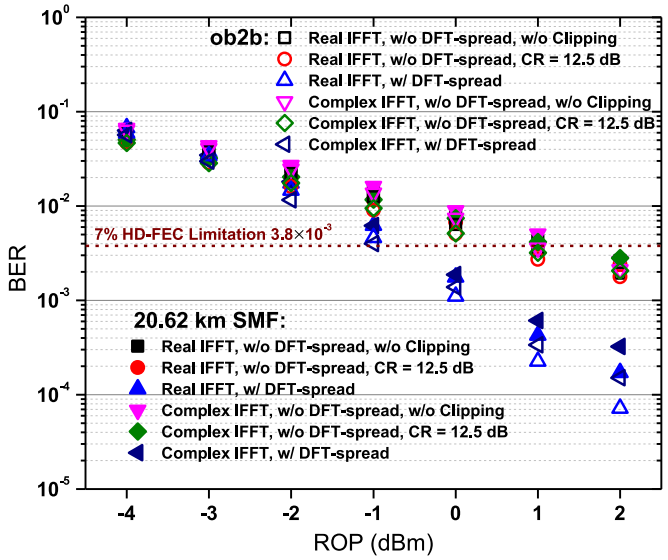

Fig. 9. Measured BER performance versus ROP for six types of OFDM signal.

V. Conclusion

The transmission performance of the proposed IFFT/FFT size efficient (complex IFFT/FFT-based) and DFT-spread enabled OFDM signal has been experimentally investigated in a DML-based IMDD SMF system. Moreover, the other five types of OFDM signal are also studied in such link for a comparison purpose. The results show that compared to the other four types of DFT-spread disabled OFDM signals, the proposed OFDM signal can achieve a PAPR reduction of 2-dB and more than 2-dB receiver sensitivity improvement at a BER of 3.8×10^{-3}. It also exhibits that the BER performance of the proposed OFDM signal is slightly worse than that of the real IFFT-based and DFT-spread enabled OFDM signal, but had lower complexity in hardware implementation and less power consumption due to the reduced IFFT/FFT size.

References

[1] S. Huang, B. Guo, X. Li, J. Zhang, Y. Zhao, and W. Gu, "Pre-configured polyhedron based protection against multi-link failures in optical mesh networks," *Opt. Exp.*, vol. 22, no. 3, pp. 2386–2402, 2014.

[2] J. Armstrong and B. J Schmidt, "Comparison of asymmetrically clipped optical OFDM and DC-biased optical OFDM in AWGN," *IEEE Commun. Lett.*, vol. 12, no. 5, pp. 343–345, May 2008.

[3] Z. Cao, J. Yu, W. Wang, L. Chen, and Z. Dong, "Direct-detection optical OFDM transmission system without frequency guard band," *IEEE Photon. Technol. Lett.*, vol. 22, no. 11, pp. 736–738, Jun. 2010.

[4] W. Shieh and C. Athaudage, "Coherent optical orthogonal frequency division multiplexing," *Electron. Lett.*, vol. 42, no. 10, pp. 587–589, 2006.

[5] X. Liu and F. Buchali, "Intra-symbol frequency-domain averaging based-channel estimation for coherent optical OFDM," *Opt. Exp.*, vol. 16, no. 26, pp. 21944–21957, 2008.

[6] Z. Cao, H. P. A. van den Boom, E. Tangdiongga, and T. Koonen, "Interleaved and partial transmission interleaved optical coherent orthogonal frequency division multiplexing," *Opt. Lett.*, vol. 39, no. 7, pp. 2179–2182, 2014.

[7] Y. Luo, X. Zhou, F. Effenberger, X. Yan, G. Peng, Y. Qian, and Y. Ma, "Time- and wavelength-division multiplexed passive optical network (TWDM-PON) for next-generation PON Stage 2 (NG-PON2)," *J. Lightw. Technol.*, vol. 31, no. 4, pp. 587–593, Feb. 2013.

[8] N. Cvijetic, "OFDM for next-generation optical access networks," *J. Lightw. Technol.*, vol. 30, no. 4, pp. 384–398, Feb. 2012.

[9] Y. Benlachtar, R. Bouziane, R. I. Killey, C. R. Berger, P. Milder, R. Koutsoyannis, J. C. Hoe, M. Pschel, and M. Glick, "Optical OFDM for the data center," in *Proc. 12th Int. Conf. Trans. Opt. Netw.*, 2010, pp. 1–4.

[10] D. Qian, N. Cvijetic, J. Hu, and T. Wang, "108 Gb/s OFDMA-PON with polarization multiplexing and direct detection," *J. Lightw. Technol.*, vol. 28, no. 4, pp. 484–493, Feb. 2010.

[11] E. Hugues-Salas, R. Giddings, X. Jin, J. Wei, X. Zheng, Y. Hong, C. Shu, and J. Tang, "Real-time experimental demonstration of low-cost VCSEL intensity-modulated 11.25Gb/s optical OFDM signal transmission over 25km PON systems," *Opt. Exp.*, vol. 19, no. 4, pp. 2979–2988, 2011.

[12] S.-H. Cho, K. W. Doo, J. H. Lee, J. Lee, S. I. Myong, and S. S. Lee, "Demonstration of a real-time 16 QAM encoded 11.52 Gb/s OFDM transceiver for IM/DD OFDMA-PON systems," presented at the 18th OptoElectronics and Communications Conf., Kyoto, Japan, 2013, Paper WP2–3.

[13] X. Xiao, F. Li, J. Yu, Y. Xia, and Y. Chen, "Real-time demonstration of 100 Gbps class dual-carrier DDO-16QAM-DMT transmission with directly modulated laser," presented at the Optical Fiber Communication Conf., San Francisco, CA, USA, 2014, Paper M2E.6.

[14] X. Q. Jin, R. P. Giddings, E. Hugues-Salas, and J. M. Tang, "Real-time demonstration of 128-QAM-encoded optical OFDM transmission with a 5.25bit/s/Hz spectral efficiency in simple IMDD systems utilizing directly modulated DFB lasers," *Opt. Exp.*, vol. 17, no. 22, pp. 20484–20493, 2009.

[15] Q. W. Zhang, E. Hugues-Salas, Y. Ling, H. B. Zhang, R. P. Giddings, J. J. Zhang, M. Wang, and J. M. Tang, "Record-high and robust 17.125 Gb/s gross-rateover 25 km SSMF transmissions of real-time dual-band optical OFDM signals directly modulated by 1 GHz RSOAs," *Opt. Exp.*, vol. 22, no. 6, pp. 6339–6348, 2014.

[16] M. Chen, J. He, and L. Chen, "Real-time optical OFDM long-reach PON system over 100-km SSMF using a directly modulated DFB laser," *IEEE/OSA J. Opt. Commun. Netw.*, vol. 6, no. 1, pp. 18–25, Jan. 2014.

[17] M. Chen, J. He, and L. Chen, "Real-time demonstration of an FPGA-based 1024-QAM OFDM transmitter in short-reach IMDD systems," *IEEE Photon. Technol. Lett.*, vol. 27, no. 8, pp. 824–827, Apr. 2015.

[18] M. Chen, J. He, Q. Fan, Z. Dong, and L. Chen, "Experimental demonstration of real-time high-level QAM-encoded direct-detection optical OFDM systems," *J. Lightw. Technol.*, vol. 33, no. 22, pp. 4632–4639, Nov. 2015.

[19] S.-Y. Jung, S.-M. Jung, and S.-K. Han, "I/Q channel separated baseband OFDM optical transmission using orthogonal polarizations in IM/DD system," *J. Lightw. Technol.*, vol. 32, no. 13, pp. 2392–2398, Jul. 2014.

[20] F. Barrami, Y. L. Guennec, E. Novakov, J.-M. Duchamp, and P. Busson, "A novel FFT/IFFT size efficient technique to generate real time optical OFDM signals compatible with IM/DD systems," in *Proc. Eur. Microw. Conf.*, Oct. 6–10, 2013, pp. 1247–1250.

[21] M. F. Sanya, L. Djogbe, A. Vianou, and C. Aupetit-Berthelemot, "DC-biased optical OFDM for IM/DD passive optical network systems," *IEEE/OSA J. Opt. Commun. Netw.*, vol. 7, no. 4, pp. 205–214, Apr. 2015

[22] Y. Tang, W. Shieh, and B. S. Krongold, "DFT-spread OFDM for fiber nonlinearity mitigation," *IEEE Photon. Technol. Lett.*, vol. 22, no. 16, pp. 1250–1252, Aug. 2010.

[23] F. Li, X. Li, J. Zhang, and J. Yu, "Transmission of 100-Gb/s VSB DFT-spread DMT signal in short-reach optical communication systems," *IEEE Photon. J.*, vol. 7, no. 5, pp. 1–7, Oct. 2015.

[24] X. Q. Jin, J. L. Wei, R. P. Giddings, T. Quinlan, S. Walker, and J. M. Tang, "Experimental demonstrations and extensive comparisons of end-to-end real-time optical OFDM transceivers with adaptive bit and/or power loading," *IEEE Photon. J.*, vol. 3, no. 3, pp. 500–511, Jun. 2011.

[25] F. Li, X. Li, L. Chen, Y. Xia, C. Ge, and Y. Chen, "High-level QAM OFDM system using DML for low-cost short reach optical communications," *IEEE Photon. Technol. Lett.*, vol. 26, no. 9, pp. 941–944, May 2014.

[26] M. Chen, J. He, J. Tang, X. Wu, and L. Chen, "Real-time 10.4-Gb/s single-band optical 256/64/16QAM receiver for OFDM-PON," *IEEE Photon. Technol. Lett.*, vol. 26, no. 20, pp. 2012–2015, Oct. 2014.

[27] Z. Feng, M. Tang, S. Fu, L. Deng, Q. Wu, R. Lin, R. Wang, P. Shum, and D. Liu, "Performance-enhanced direct detection optical OFDM transmission with CAZAC equalization," *IEEE Photon. Technol. Lett.*, vol. 27, no. 14, pp. 1507–1510, Jul. 2015.

Authors' biographies not available at the time of publication.